Title

Multiconfigurational Electronic Structure of Nickel Cross-Coupling Catalysts Revealed by X-ray Absorption Spectroscopy.

Authors

Nelson, Kacie

Kazmierczak, Nathanael

Cagan, David

et al.

Publication Date

2024-12-19

DOI

10.1021/acs.jpclett.4c02917

Peer reviewed

THE JOURNAL OF PHYSICAL CHEMISTRY LETTERS
A JOURNAL OF THE AMERICAN CHEMICAL SOCIETY

pubs.acs.org/JPCL
Letter

Multiconfigurational Electronic Structure of Nickel Cross-Coupling Catalysts Revealed by X-ray Absorption Spectroscopy

Kacie J. Nelson, Nathanael P. Kazmierczak, David A. Cagan, Alec H. Follmer, Thais R. Scott, Sumana L. Raj, Douglas Garratt, Natalia Powers-Riggs, Kelly J. Gaffney, Ryan G. Hadt,* and Amy A. Cordones*

Cite This: J. Phys. Chem. Lett. 2025, 16, 87−94
Read Online

ACCESS | Metrics & More | Article Recommendations | Supporting Information

ABSTRACT: Ni^{II} 2,2′-bipyridine complexes are commonly invoked intermediates in metallaphotoredox cross-coupling reactions. Despite their ubiquity, design principles targeting improved catalytic performance remain underdetermined. A series of Ni(^{R}bpy)($^{R'}$Ar)Cl (R = MeOOC, *t*-Bu, R′ = CH_3, CF_3) complexes were proposed to have multiconfigurational electronic structures on the basis of multiconfigurational/multireference calculations, with significant mixing of Ni → bpy metal-to-ligand charge transfer (MLCT) configurations into the ground-state wave function. Here, Ni K-edge and $L_{2,3}$-edge X-ray absorption spectroscopies provide experimental support for the highly covalent and multiconfigurational electronic structures of these complexes. The pre-edge intensity in the K-edge spectrum reflects highly covalent Ni−aryl bonding. The L_3-edge spectral shape is dependent on ligand functionalization, and a feature reflecting the MLCT character is assigned using prior *ab initio* and new semiempirical calculations. The results suggest the push/pull effects of the aryl/bpy ligands moderate the changes in electron density on Ni during the multiredox cross-coupling reaction cycle.

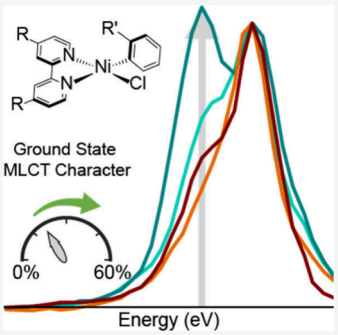

Metallaphotoredox catalysis activates 3*d* transition metals to accomplish challenging synthetic transformations important to drug synthesis and development.[1−3] Due to their ability to perform $1e^-$ redox processes and radical capture, first-row transition metals can display reactivities distinct from their 4*d* and 5*d* counterparts. Nickel 2,2′-bipyridine aryl halide (Ni(bpy)ArX) complexes (such as those shown in Figure 1a) are a common motif in metallaphotoredox catalysis, having been implicated as precatalysts or catalysts in cross-coupling schemes for a variety of substrates. The proposed role of Ni(bpy)ArX complexes is substrate-specific, with ground-,[4,5] excited-state,[6] and redox chemistries[7] all being proposed modes of reactivity.[2,8] A handful of kinetic studies have provided experimental evidence for some mechanisms,[9,10] but the wide array of proposed reactivities and incomplete understanding of the electronic structure of this class of complexes has made the identification of design principles difficult.

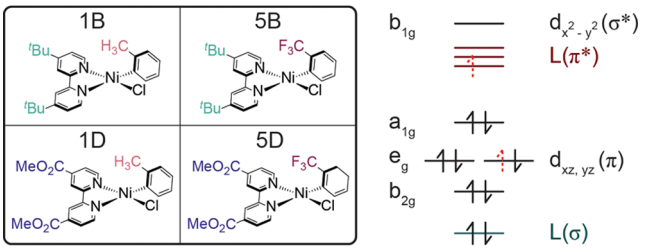

Figure 1. (a) Molecular structures of the Ni(bpy)ArCl complexes examined in this Letter (numbering scheme from ref 16). (b) Illustration of the molecular orbital picture of these complexes previously determined by *ab initio* calculations (ref 16). Red dotted arrows indicate partial orbital occupancy.

Ligand design is important to the valence electronic structure and reactivity of transition metal cross-coupling catalysts.[11] Understanding metal−ligand covalency is particularly important for first-row transition metals, as these interactions can challenge traditional oxidation state formalisms, redistribute charge across a molecule in the ground state, and modify excited-state pathways.[12−14] Ni(bpy)ArX complexes are square planar in geometry with a low-spin singlet d^8 configuration (Figure 1b).[8] Density functional theory (DFT) calculations predict a highly covalent Ni−aryl bond, with the nominally metal-centered $d_{x^2-y^2}$ valence orbital being calculated to possess only ∼53% Ni *d*-character.[6,15,16] Multiconfigurational complete active space self-consistent field (CASSCF)

Received: October 8, 2024
Revised: November 15, 2024
Accepted: December 5, 2024
Published: December 19, 2024

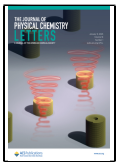

https://doi.org/10.1021/acs.jpclett.4c02917
J. Phys. Chem. Lett. 2025, 16, 87−94

calculations performed on a family of these molecules further posit that their electronic ground states possess significant Ni → bpy metal-to-ligand charge transfer (MLCT) character mixed with the d^8 configuration.[15,16] The extent of MLCT mixing varies upon substitution of the bpy and aryl ligands with electron-donating or -withdrawing groups. The rationale for this behavior is similar to what is known in ligand field theory as π- backbonding, which is primarily driven by the energetic separation and spatial overlap between occupied metal d-orbitals and unoccupied ligand π^* orbitals of appropriate symmetry. Electron-donating groups on the bpy ligand (complexes **1B** and **5B**, Figure 1a) destabilize the π^* manifold relative to the occupied d-manifold, resulting in less predicted MLCT character. Electron-donating groups on the aryl ligand (complexes **1D** and **1B**, Figure 1a) increase the strength of σ-donation to the metal center, thus destabilizing the Ni d-manifold, resulting in more predicted MLCT character. The predicted MLCT character in the ground state correlates with the quantum yield of excited-state Ni−C bond homolysis, a commonly proposed initiation step in Ni^{II}-based metallaphotoredox catalysis.[16] However, no direct experimental evidence has validated the predicted multiconfigurational electronic structure of these complexes to date. This link between Ni−C bond homolysis activity and predicted metal−ligand interactions motivates the experimental investigation of the valence electronic structure with the X-ray spectroscopies presented herein.

This work presents Ni K-edge and $L_{2,3}$-edge X-ray absorption spectroscopies (XAS) to probe the valence electronic structure of the series of Ni(bpy)ArCl complexes **1D**, **1B**, **5D**, and **5B** in Figure 1a (a subset of the Ni(bpy)ArCl complexes previously reported[16]) and provides experimental support for their predicted covalent and multiconfigurational character.[16] Core-level spectroscopies at the metal edge report specifically on the electronic and structural properties of the metal center. By probing the spatial overlap of the highly localized core orbitals and valence orbitals, these spectroscopies directly probe the metal−ligand covalency. Ni $L_{2,3}$-edge spectroscopy, in particular, is sensitive to spin state[17,18] and metal 3d-character in unoccupied valence orbitals,[19] such that electronic changes to the metal center due to multiconfigurational ground-state character can be probed.[20] In conjunction with the prior CASSCF electronic structure calculations and newly presented time-dependent DFT and charge-transfer multiplet spectral simulations, we demonstrate a direct link between observed K-edge and $L_{2,3}$-edge XAS spectral features and the highly covalent and multiconfigurational electronic structure of Ni(bpy)ArCl complexes.

The Ni K-edge XAS data of complex **1D** and a square planar low-spin Ni^{II} reference (Ni phthalocyanine, NiPc)[21,22] are presented in Figure 2a,b. The measurement details are reported in Supporting Information Section 1.3. The pre-edge and rising-edge regions are highlighted in panel b. Excitations in these regions correspond to transitions of Ni 1s electrons to unoccupied valence orbitals with Ni 3d and 4p character via quadrupole- and dipole-allowed transitions, respectively, and are sensitive probes of both geometric and electronic structure. The intense rising-edge feature (8338.2 eV for **1D**, 8340.0 eV for NiPc) is a hallmark of the square planar geometry, attributed to a stabilized 1s → 4p_z transition.[23] Notably, both the 1s → 4p_z transition and edge-jump of **1D** are red-shifted in comparison to NiPc by 1.8 and 2.1 eV, respectively, indicative of the reduced effective nuclear

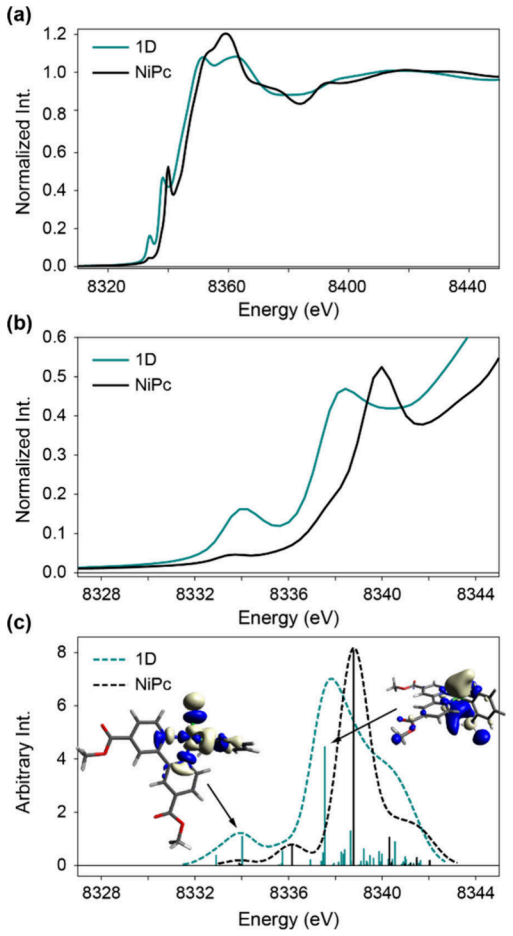

Figure 2. (a) Ni K-edge XAS of **1D** and low-spin reference Ni^{II} phthalocyanine (NiPc). (b) Pre-edge region of the Ni XAS spectra demonstrating increased pre-edge peak intensity for **1D**. (c) TD-DFT spectral simulations. Molecular orbitals represent the transition orbital for the highest intensity stick in the pre-edge and rising-edge regions, respectively (iso value = 0.03).

charge (Z_{eff}) at the metal center expected in the presence of the strongly donating aryl ligand (Table S4).[23]

The pre-edge 1s → 3d features (8333.9 eV for **1D**, 8333.5 eV for NiPc) are typically 2 orders of magnitude weaker than the dipole-allowed 1s → 4p transitions but can gain significant intensity from minor amounts of 3d/4p orbital mixing.[24] We note that the pre-edge peak is both blue-shifted and nearly an order of magnitude more intense for **1D** than that observed for NiPc and other low-spin Ni^{II} square planar complexes (Table S4).[23,25,26] The shift of **1D** to higher energy is accordant with possessing a larger ligand field splitting, likely due to the incorporation of the strong-field aryl ligand. The unusually high intensity of the **1D** pre-edge feature is found to be consistent with that of other Ni−C bonded complexes. We report the Ni K-edge spectrum of [(TMEDA)Ni^{II}(o-tolyl)Cl] (TMEDA = tetreamethylethylenediamine) in Figure S2, which has a similarly intense pre-edge feature but does not contain bipyridyl ligands, indicating the necessity of the Ni−aryl bond. Furthermore, a strong pre-edge has previously been reported for Ni−mesityl complexes[27,28] and other organonickel species.[12,29]

The origin of the intense pre-edge feature of **1D** is revealed by time-dependent density functional theory (TD-DFT) calculations and can be linked to differences in both the

https://doi.org/10.1021/acs.jpclett.4c02917
J. Phys. Chem. Lett. 2025, 16, 87−94

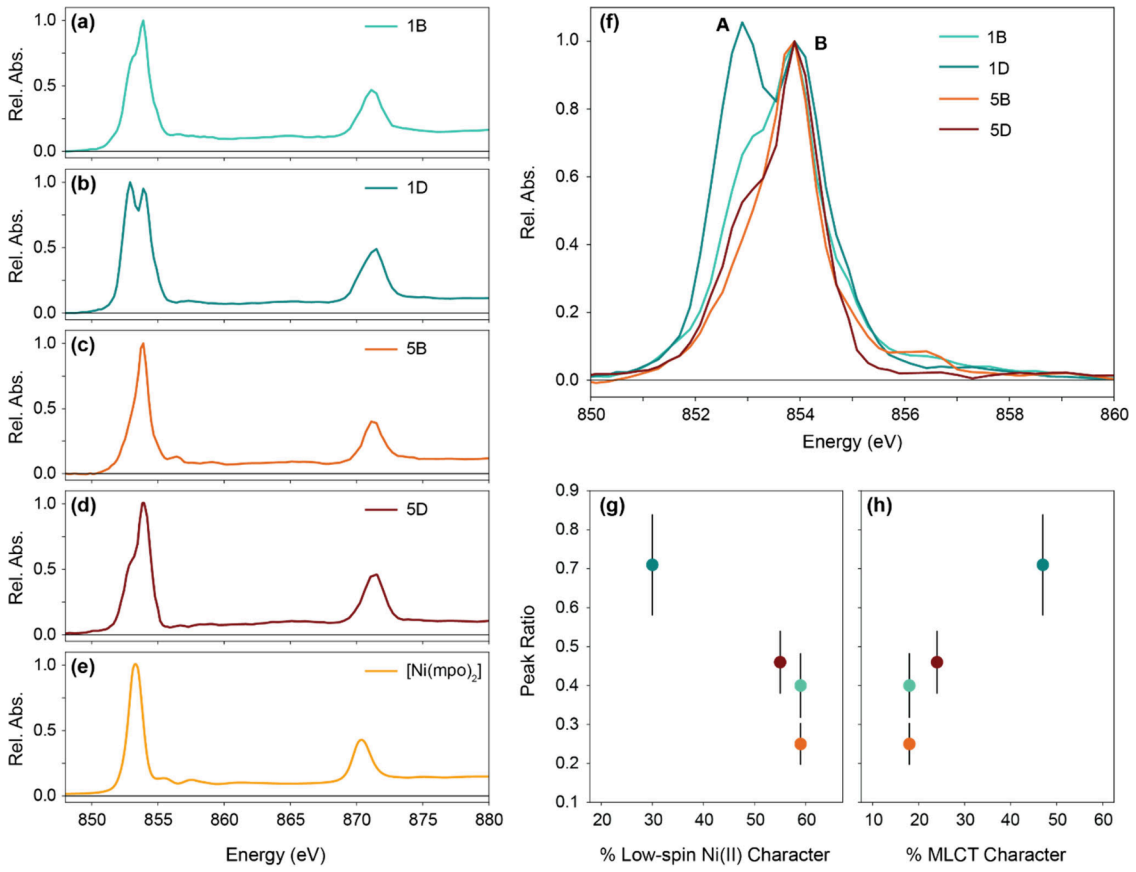

Figure 3. Ni $L_{2,3}$-edge spectra for the Ni^{II} series **1B** (a), **1D** (b), **5B** (c), and **5D** (d) and reference Ni^{II} low-spin $[Ni(mpo)_2]$[38] (e). (f) Overlaid edge-jump subtracted and normalized L_3-edge spectra of Ni^{II} series demonstrates change in relative intensity of Peak A with ligand modification. (g) Plot of peak ratio vs CASSCF/QD-NEVPT2 calculated singlet Ni^{II} character from ref 16 in the ground-state wave function and (h) peak ratio vs CASSCF/QD-NEVPT2 calculated MLCT (Ni → bpy) character in the ground-state wave function. Peak ratio is defined as the area under Peak A divided by the area under Peak B.

electronic structure and coordination geometry induced by Ni−C bonding. The computed spectra are shown in Figure 2c, and the computational methods are described in Supporting Information Section 1.5. The intensity of the pre-edge region is primarily derived from two transitions that are not resolved experimentally. The lower-energy, lower-intensity transition at 8332.8 eV is to an unoccupied orbital of primarily bpy character with minor Ni 3*d* (7.7%) and $4p_z$ (1.6%) mixing (see Figure S6 "LUMO"). The unoccupied orbital underlying the higher-intensity transition in the pre-edge peak (8333.9 eV) of **1D** has significant Ni $3d_{x^2-y^2}$ character with some $4p_x$ hybridization (1.6%, see Figure S6 "LUMO+3"). The mixing of Ni *p* character into the $3d_{x^2-y^2}$ orbital is considerably higher than predicted for NiPc (<0.1% Ni *p* character), resulting in the large increase in peak intensity for **1D**.

The increased 3*d*/4*p* mixing observed in **1D** has both electronic and structural origins. Unlike NiPc and other highly symmetric square planar complexes, the symmetry of Ni(bpy)-ArX complexes is not well-approximated by the D_{4h} point group. Previously reported crystal structures of **1D**[30] of **1B**[6] and our own DFT geometry optimized structures indicate that the Ni−C_{aryl} bond is shorter than the trans Ni−N_{bpy} bond by ∼0.1 Å, such that 3*d*/4*p* mixing becomes symmetry-allowed (Table S5). Additionally, a commonly proposed model for 3*d*/4*p* mixing suggests that the interaction is mediated via overlap with ligand 2*p* orbitals, i.e., via metal−ligand covalency.[31,32] Both the metal $d_{x^2-y^2}$ and p_x orbitals contributing to the larger pre-edge transition can mix with ligand orbitals of p_x symmetry to generate a covalent molecular orbital of mixed character. Indeed, analysis of the MOs generated by DFT reveals that the antibonding Ni $d_{x^2-y^2}$ orbital of complex **1D** possesses only 49.7% Ni *d* character, with 20.3% aryl character. The higher covalency reported here as compared to previously published DFT calculations[6,16] is likely due to a change in functional from B3LYP (20% exact exchange) to nonhybrid TPSS (0% exact exchange).[33,34] Nonetheless, both functionals indicate a high covalency of the $d_{x^2-y^2}$ orbital. Thus, the high-intensity pre-edge peak of **1D** also acts as a direct, though not quantitative, observation of the Ni−aryl covalency proposed previously.[6,15,16] DFT suggests similar degrees of Ni−aryl covalency and 4*p*/3*d* mixing across the series **1D**, **1B**, **5D**, and **5B** (Table S6).

While the above K-edge spectral features are found to be sensitive to the presence of the Ni-aryl versus Ni−N_4 covalency, we do not see a large effect of Ni 3*d*-bpy interactions on the K-edge spectrum (as indicated by the similarity between [(TMEDA)Ni^{II}(*o*-tolyl)Cl] and **1D**). To assess claims of metal → bpy MLCT character in the ground-state electronic structure, we therefore turn to the Ni $L_{2,3}$-edge XAS. Metal $L_{2,3}$-edge XAS probes dipole-allowed metal 2*p* → 3*d* transitions and is directly sensitive to metal *d*-character in unoccupied valence orbitals.[19,24] Metal $L_{2,3}$-edge spectra are heavily influenced by spin−orbit coupling in the *p*- and *d*-manifolds, as well as exchange and correlation between the *p*

https://doi.org/10.1021/acs.jpclett.4c02917
J. Phys. Chem. Lett. 2025, 16, 87−94

and d holes in the core-excited state. These multibody effects give rise to multiplet features and make $L_{2,3}$-edge spectra challenging to interpret but information-rich. Transition metal $L_{2,3}$-edge spectroscopy has been used to quantitively assess metal−ligand covalency[19,24] and to elucidate electronic structures that are difficult to assess with other techniques, such as mixed-spin[20] and highly π-backbonding configurations.[35−37]

The Ni $L_{2,3}$-edge spectra of **1D**, **1B**, **5D**, and **5B** are shown in Figure 3a−d, with a low-spin Ni^{II} reference[38] spectrum in panel e. The measurement details are reported in Supporting Information Section 1.4. The L_3-edge spectra of all reported Ni(bpy)ArCl complexes show two distinct features, labeled Peak A (852.91 eV for **1B**) and Peak B (853.89 eV for **1B**), with relative intensities dependent on ligand substituent group. Peak positions vary between complexes by less than 0.2 eV for Peak A and 0.15 eV for Peak B (Table S7). The spectrum of **1B** is consistent with that reported previously by Wallick et al.[39]

The presence of two strong peaks in the Ni L_3 spectrum is inconsistent with other low-spin Ni^{II} complexes reported previously,[12,17,26,29,38,40,41] which characteristically exhibit a single dominant peak due to a $2p \rightarrow 3d_{x^2-y^2}$ orbital transition, with only minor multiplet contributions (Figure 3e, for example). The L_3-edge peak maximum of low-spin formally Ni^{II} complexes typically appears in the range of 853−854 eV and is influenced by the ligand field and oxidation state of the metal center.[12,17,38] The observed maximum of Peak B for the **1D**−**5B** Ni(bpy)ArCl series is at the high end of this range and is consistent with previous reports of organonickel complexes.[12,29] Because of the energy and relatively high intensity of Peak B for all four complexes, we tentatively assign this feature to transitions from a $2p^6b_{2g}{}^2e_g{}^4a_{1g}{}^2b_{1g}{}^0$ initial configuration to a $2p^5b_{2g}{}^2e_g{}^4a_{1g}{}^2b_{1g}{}^1$ excited-state configuration.

The assignment of Peak A requires more explanation as an analogous feature is not present in other low-spin Ni^{II} spectra to our knowledge. The relative intensity of Peak A compared to Peak B is sensitive to functionalization of the bpy and aryl ligands, indicating that Peak A is sensitive to either (a) metal−ligand covalency or (b) ligand field strength. We compare the previously calculated[16] (CASSCF/QD-NEVPT2) multiconfigurational properties of the Ni(bpy)ArCl series to the relative intensity of Peak A to identify ground-state properties that correlate with the emergence of this peak. The Peak A:Peak B ratios plotted in Figure 3g,h are determined by fitting each L_3-edge spectrum to a two pseudo-Voigt model (Table S7, Figure S7). The relative intensity of Peak A is anticorrelated with the calculated ground-state singlet d^8 character (Figure 3g). It is also anticorrelated with the calculated ^1d-d state character (Figure S8). Furthermore, the Evans method does not indicate significant paramagnetism in the ground state (Supporting Information Section 1.2), such that significant contribution of a triplet ^3d-d configuration to the ground-state electronic structure is not considered here as a viable explanation for the observed spectral changes. Instead, we find that the appearance of Peak A is positively correlated with the calculated Ni → bpy MLCT character (Figure 3h). Thus, we posit that increasing amounts of the ground-state MLCT configuration result in the appearance of this second strong peak.

The mixing of MLCT character into the ground-state wave function is related to the degree of π-backbonding in the complex. In a classical ligand field theory picture of backbonding, occupied metal-centered d_{xz} or d_{yz} orbitals have the correct symmetry to mix with unoccupied, high-energy π^* orbitals on the bpy ligand. The resulting molecular orbitals contain partial electron transfer to the ligand through the π framework. In a CASSCF calculation, ground-state interactions between the metal-centered d orbitals and the ligand-based π^* orbitals may occur through two mechanisms: (i) the active space orbitals themselves may become delocalized over the metal−ligand bond, or (ii) multiple configurations may contribute to the ground state, while the orbitals remain localized to the metal and ligand centers. Varying the number of excited states included in the CASSCF calculation can also affect active orbital shapes and occupations. In the case of MLCT mixing where the configuration features a $d_{xz}/d_{yz} \rightarrow$ bpy π^* orbital transition (such as in the case of **1B**−**5D**), mechanisms (i) and (ii) both arise from the same type of orbital interaction that is described by backbonding in ligand field theory.

Previous literature has demonstrated that π-backbonding can generate intense secondary peaks in L_3-edge spectra of octahedral Fe^{II} and Ru^{II} complexes.[35,42] In these cases, the main L_3 absorption feature constitutes transitions from $2p \rightarrow 3d(e_g^*)$, but the presence of backbonding results in additional transitions described by an overall $2p \rightarrow \pi^*(L)$ excitation due to the admixture of metal d-character. In $[Fe(CN)_6]^{4-}$, these transitions produce an intense peak at higher energy than the main $2p \rightarrow 3d(e_g^*)$ transition, on account of the higher energy of the $\pi^*(L)$ orbitals relative to that of the $3d(e_g^*)$ orbitals. However, in the Ni(bpy)ArCl complexes investigated here, it has been argued that the bpy π^* acceptor orbitals lie at lower energy than the unoccupied $d_{x^2-y^2}$ orbital.[16] We therefore hypothesize that π-backbonding in **1B**−**5D** results in a transition featuring bpy π^* acceptor orbitals at a lower energy than the main $2p \rightarrow 3d$ absorption. This would explain the increasing intensity of Peak A with increasing MLCT character.

Charge transfer multiplet (CTM) simulations have successfully modeled the satellite peaks arising from backbonding in Fe complexes.[35] In a multiplet simulation, localized metal and ligand orbitals are assumed, and backbonding is modeled by matrix element mixing of configurations with different occupations of these localized orbitals. Thus, multiplet simulations conform closely to the CASSCF description of a ground-state multiconfigurational wave function. Previous work on 1B has shown that a split L_3-edge may indeed be simulated through the use of multiplet simulations.[39] However, due to the large number of empirical parameters used in CTM calculations, tuning those parameters to produce the best match to the experiment does not necessarily yield a unique solution.

We adopted a different approach to tuning the multiplet simulation parameters, seeking to make the semiempirical Hamiltonian adhere as closely as possible to known information about the ground and valence excited states of **1B**−**5D**. This maximizes the physical plausibility of the multiplet model. Simulations employed the Quanty language,[43−47] with the Crispy graphical user interface[48] used for some simulations. A detailed description of the CTM simulation parameters can be found in Supporting Information Sections 1.6 and 4. Briefly, the empirical crystal field and Coulomb repulsion parameters were tuned until the resulting predicted valence $d-d$ excitations best match those calculated by TD-DFT[16] (Table S2). The energies of the ligand orbitals involved in the charge transfer mixing were constrained to lie

https://doi.org/10.1021/acs.jpclett.4c02917
J. Phys. Chem. Lett. 2025, 16, 87−94

above the occupied *d*-orbitals. Finally, only a single MLCT mixing parameter $T(e_g)$ is introduced, restricting the symmetry to specifically simulate the π-backbonding interaction (Table S3).

By tuning $T(e_g)$, the amount of MLCT mixing into the ground and excited states can be rationally adjusted and the systematic effects on the Ni L_3-edge spectrum can be elucidated. When increasing the magnitude of $T(e_g)$, we observe a splitting in the L_3-edge (Figure 4A). A new peak

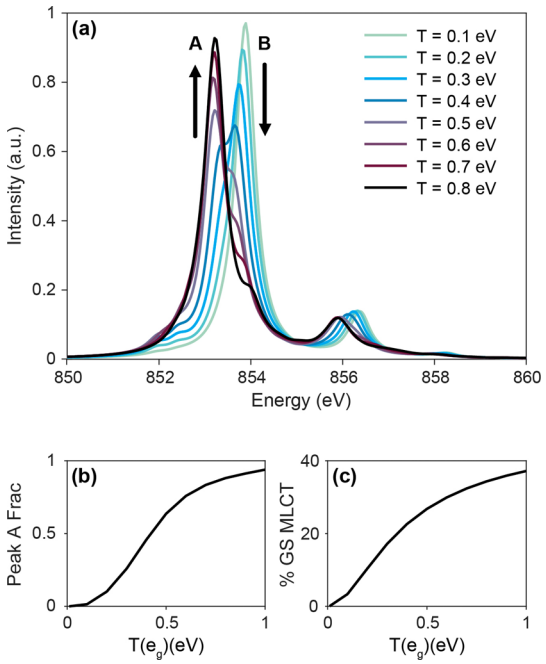

Figure 4. Semiempirical multiplet simulations of Ni(bpy)ArCl L_3 edge spectra. (a) Splitting of the L_3-edge into two peaks is controlled by variation of the π-backbonding strength, $T(e_g)$. (b) Increased backbonding leads to a larger contribution of Peak A to the total L_3-edge peak intensity. (c) Increased backbonding leads to a larger amount of ground-state MLCT character.

(labeled Peak A) grows in at lower energies, qualitatively matching the experimental L_3-edge spectra in the range $T(e_g)$ < 0.4 eV. This splitting is not observed if mixing to the σ-symmetry orbital is applied, $T(b_{1g})$ (Figure S10). As in the experimental spectra, these two peaks retain reasonably similar energy positions, shifting in the simulation by only ~0.3 eV over the full range of $T(e_g)$ values. As $T(e_g)$ is increased, the ground state acquires more MLCT multiconfigurational character, as quantified by the occupation number of the ligand acceptor orbitals in the ground-state wave function (Figure 4C). When the peaks reach equal height ($T(e_g)$ = 0.4 eV), the ground state acquires 23% MLCT character. This qualitatively captures the expected trend: the appearance and increasing relative intensity of Peak A indicate a greater degree of multiconfigurational MLCT character, indicating a stronger backbonding interaction. A more quantitative consideration of the limitations of this CTM model can be found in Supporting Information Section 4.

The results presented here provide the first experimental support for the multiconfigurational electronic structure of Ni(bpy)ArCl complexes.[16] The results thus demonstrate a direct link between the ground-state multiconfigurational character of the catalysts and their quantum yield of photochemical Ni−C bond homolysis,[16] elucidating a design principle for the desired photochemical behavior. The combination of Ni K-edge and L_3-edge spectroscopies demonstrates that the Ni−aryl complexes possess a bonding scheme that is highly σ-covalent and π-backbonding. TD-DFT, which accurately reproduces the Ni K-edge spectrum, predicts that nearly half of the $d_{x^2-y^2}$ electron hole of the ground state is delocalized over the ligand manifold. Such high degrees of ligand character in nominally metal-centered orbitals is typically invoked for formally high valent, late transition metal centers like Cu^{III} and Ni^{IV}[12,13,49] or in the case of strongly σ-donating ligands such as sulfur-coordinating dithiolenes.[38,50] This σ-noninnocence has even been proposed to facilitate a Ni^{II}/Ni^{IV} catalyzed cross-coupling mechanism, where the Ni center modulates the ligand charge instead of vice versa.[51] If the aryl ligand pushes charge onto the Ni center of the Ni(bpy)ArX series, the backbonding interaction proposed on the basis of the L_3-edge spectroscopy represents a mechanism by which charge is pulled from the metal center by the bpy ligand. Redox noninnocent π^* manifolds have been characterized in a number of related Ni(diimine)−aryl species and are proposed to mediate charge at the Ni center in some cross-coupling mechanisms.[52−56]

These findings indicate that this series of Ni(bpy)ArX complexes show interligand electron pushing mediated by the metal center, similar to the mechanism by which carbonyl stretching frequencies are changed by phosphine ligands in the Tolman electronic parameter series.[57] Beyond photolytic Ni−C bond cleavage, this ligand interplay may contribute to the reactivity of the complexes by moderating the changes in electron density on the Ni center during a multiredox reaction cycle. For example, Ni(bpy)ArCl complexes are proposed to undergo Ni−C bond homolysis to enter a dark Ni^{I}/Ni^{III} cycle, where metal−ligand interactions may factor into the reactivity of the intermediates.[6] Indeed, it has already been demonstrated that the electron-donating/-withdrawing character of the bpy ligand has a strong effect on the reactivity of Ni^{I}−bpy complexes toward oxidative addition by modulating the Z_{eff} of the metal center.[58] Overall, these results indicate that Ni(bpy)ArX complexes possess highly covalent Ni−C bonds as well as significant multiconfigurational Ni → bpy mixing into the ground state. This mixing may impact their reactivity and indicate that metal−ligand interactions are an important component for understanding Ni^{II} metallaphotoredox mechanisms.

■ ASSOCIATED CONTENT

Supporting Information

The Supporting Information is available free of charge at https://pubs.acs.org/doi/10.1021/acs.jpclett.4c02917.

Methods; Ni K-edge XAS supporting figures and tables, including DFT and TD-DFT results and spectral simulations; Ni L-edge XAS additional figures and tables; and further CTM Ni L-edge XAS simulation results (PDF)

Transparent Peer Review report available (PDF)

■ AUTHOR INFORMATION

Corresponding Authors

Ryan G. Hadt − *Division of Chemistry and Chemical Engineering, Arthur Amos Noyes Laboratory of Chemical Physics, California Institute of Technology, Pasadena,*

https://doi.org/10.1021/acs.jpclett.4c02917
J. Phys. Chem. Lett. 2025, 16, 87−94

California 91125, United States; orcid.org/0000-0001-6026-1358; Email: rghadt@caltech.edu

Amy A. Cordones − *Stanford PULSE Institute, SLAC National Accelerator Laboratory, Stanford University, Menlo Park, California 94025, United States;* orcid.org/0000-0001-9897-5380; Email: acordon@slac.stanford.edu

Authors

Kacie J. Nelson − *Stanford PULSE Institute, SLAC National Accelerator Laboratory, Stanford University, Menlo Park, California 94025, United States*

Nathanael P. Kazmierczak − *Division of Chemistry and Chemical Engineering, Arthur Amos Noyes Laboratory of Chemical Physics, California Institute of Technology, Pasadena, California 91125, United States;* orcid.org/0000-0002-7822-6769

David A. Cagan − *Division of Chemistry and Chemical Engineering, Arthur Amos Noyes Laboratory of Chemical Physics, California Institute of Technology, Pasadena, California 91125, United States;* orcid.org/0000-0002-4719-2789

Alec H. Follmer − *Division of Chemistry and Chemical Engineering, Arthur Amos Noyes Laboratory of Chemical Physics, California Institute of Technology, Pasadena, California 91125, United States;* orcid.org/0000-0002-6244-6804

Thais R. Scott − *Division of Chemistry and Chemical Engineering, Arthur Amos Noyes Laboratory of Chemical Physics, California Institute of Technology, Pasadena, California 91125, United States*

Sumana L. Raj − *Stanford PULSE Institute, SLAC National Accelerator Laboratory, Stanford University, Menlo Park, California 94025, United States;* orcid.org/0000-0001-5570-3350

Douglas Garratt − *Linac Coherent Light Source (LCLS), SLAC National Accelerator Laboratory, Menlo Park, California 94025, United States;* orcid.org/0000-0002-8637-9984

Natalia Powers-Riggs − *Stanford PULSE Institute, SLAC National Accelerator Laboratory, Stanford University, Menlo Park, California 94025, United States;* orcid.org/0000-0002-9309-9622

Kelly J. Gaffney − *Stanford PULSE Institute, SLAC National Accelerator Laboratory, Stanford University, Menlo Park, California 94025, United States;* orcid.org/0000-0002-0525-6465

Complete contact information is available at: https://pubs.acs.org/10.1021/acs.jpclett.4c02917

Notes

The authors declare no competing financial interest.

■ ACKNOWLEDGMENTS

Research supported as part of BioLEC, an Energy Frontier Research Center funded by the U.S. Department of Energy (DOE), Office of Science, Basic Energy Sciences (BES), under Award # DE-SC0019370. Work by D.G. and N.P.-R. was supported by the U.S. Department of Energy, Office of Basic Energy Sciences, Division of Chemical Sciences, Geosciences and Biosciences, through SLAC National Accelerator Laboratory under Contract No. DE-AC02-76SF00515. D.A.C. and N.P.K. both acknowledge support from National Science Foundation Graduate Research Fellows (DGE-1745301). D.A.C. is also supported by a National Academies of Science, Engineering, and Medicine Ford Foundation Predoctoral Fellowship, while N.P.K. is also supported by the Hertz Fellowship. T.R.S. was supported by the Presidential Postdoctoral Fellowship by the California Institute of Technology. R.G.H. acknowledges support by the National Institutes of Health (National Institute of General Medical Sciences, R35-GM142595). Use of the Stanford Synchrotron Radiation Lightsource, SLAC National Accelerator Laboratory, is supported by the U.S. Department of Energy, Office of Science, Office of Basic Energy Sciences under Contract No. DE-AC02-76SF00515. This research used resources of the Advanced Light Source, which is a DOE Office of Science User Facility under contract no. DE-AC02-05CH11231. Some of the computing for this project was performed on the Sherlock cluster. We would like to thank Stanford University and the Stanford Research Computing Center for providing computational resources and support that contributed to these research results.

■ REFERENCES

(1) Tellis, J. C.; Primer, D. N.; Molander, G. A. Single-Electron Transmetalation in Organoboron Cross-Coupling by Photoredox/Nickel Dual Catalysis. *Science* **2014**, *345* (6195), 433−436.

(2) Chan, A. Y.; Perry, I. B.; Bissonnette, N. B.; Buksh, B. F.; Edwards, G. A.; Frye, L. I.; Garry, O. L.; Lavagnino, M. N.; Li, B. X.; Liang, Y.; Mao, E.; Millet, A.; Oakley, J. V.; Reed, N. L.; Sakai, H. A.; Seath, C. P.; MacMillan, D. W. C. Metallaphotoredox: The Merger of Photoredox and Transition Metal Catalysis. *Chem. Rev.* **2022**, *122* (2), 1485−1542.

(3) Zuo, Z.; Ahneman, D. T.; Chu, L.; Terrett, J. A.; Doyle, A. G.; MacMillan, D. W. C. Merging Photoredox with Nickel Catalysis: Coupling of α-Carboxyl sp^3-carbons with Aryl Halides. *Science* **2014**, *345* (6195), 437−440.

(4) Cusumano, A. Q.; Chaffin, B. C.; Doyle, A. G. Mechanism of Ni-Catalyzed Photochemical Halogen Atom-Mediated C(sp^3)−H Arylation. *J. Am. Chem. Soc.* **2024**, *146* (22), 15331−15344.

(5) Welin, E. R.; Le, C.; Arias-Rotondo, D. M.; McCusker, J. K.; MacMillan, D. W. C. Photosensitized, Energy Transfer-Mediated Organometallic Catalysis through Electronically Excited Nickel(II). *Science* **2017**, *355* (6323), 380−385.

(6) Shields, B. J.; Kudisch, B.; Scholes, G. D.; Doyle, A. G. Long-Lived Charge-Transfer States of Nickel(II) Aryl Halide Complexes Facilitate Bimolecular Photoinduced Electron Transfer. *J. Am. Chem. Soc.* **2018**, *140* (8), 3035−3039.

(7) Shields, B. J.; Doyle, A. G. Direct C(sp^3)−H Cross Coupling Enabled by Catalytic Generation of Chlorine Radicals. *J. Am. Chem. Soc.* **2016**, *138* (39), 12719−12722.

(8) Cagan, D. A.; Bím, D.; Kazmierczak, N. P.; Hadt, R. G. Mechanisms of Photoredox Catalysis Featuring Nickel−Bipyridine Complexes. *ACS Catal.* **2024**, *14* (11), 9055−9076.

(9) Ben-Tal, Y.; Lloyd-Jones, G. C. Kinetics of a Ni/Ir-Photocatalyzed Coupling of ArBr with RBr: Intermediacy of $ArNi^{II}(L)Br$ and Rate/Selectivity Factors. *J. Am. Chem. Soc.* **2022**, *144* (33), 15372−15382.

(10) Till, N. A.; Tian, L.; Dong, Z.; Scholes, G. D.; MacMillan, D. W. C. Mechanistic Analysis of Metallaphotoredox C−N Coupling: Photocatalysis Initiates and Perpetuates Ni(I)/Ni(III) Coupling Activity. *J. Am. Chem. Soc.* **2020**, *142* (37), 15830−15841.

(11) Lundgren, R. J.; Stradiotto, M. Addressing Challenges in Palladium-Catalyzed Cross-Coupling Reactions Through Ligand Design. *Chem.—Eur. J.* **2012**, *18* (32), 9758−9769.

(12) DiMucci, I. M.; Titus, C. J.; Nordlund, D.; Bour, J. R.; Chong, E.; Grigas, D. P.; Hu, C.-H.; Kosobokov, M. D.; Martin, C. D.; Mirica, L. M.; Nebra, N.; Vicic, D. A.; Yorks, L. L.; Yruegas, S.; MacMillan, S. N.; Shearer, J.; Lancaster, K. M. Scrutinizing Formally Ni^{IV} Centers

through the Lenses of Core Spectroscopy, Molecular Orbital Theory, and Valence Bond Theory. *Chem. Sci.* **2023**, *14* (25), 6915−6929.
(13) DiMucci, I. M.; Lukens, J. T.; Chatterjee, S.; Carsch, K. M.; Titus, C. J.; Lee, S. J.; Nordlund, D.; Betley, T. A.; MacMillan, S. N.; Lancaster, K. M. The Myth of d^8 Copper(III). *J. Am. Chem. Soc.* **2019**, *141* (46), 18508−18520.
(14) Wenger, O. S. Photoactive Complexes with Earth-Abundant Metals. *J. Am. Chem. Soc.* **2018**, *140* (42), 13522−13533.
(15) Cagan, D. A.; Stroscio, G. D.; Cusumano, A. Q.; Hadt, R. G. Multireference Description of Nickel−Aryl Homolytic Bond Dissociation Processes in Photoredox Catalysis. *J. Phys. Chem. A* **2020**, *124* (48), 9915−9922.
(16) Cagan, D. A.; Bím, D.; Silva, B.; Kazmierczak, N. P.; McNicholas, B. J.; Hadt, R. G. Elucidating the Mechanism of Excited-State Bond Homolysis in Nickel−Bipyridine Photoredox Catalysts. *J. Am. Chem. Soc.* **2022**, *144* (14), 6516−6531.
(17) Wang, H.; Butorin, S. M.; Young, A. T.; Guo, J. Nickel Oxidation States and Spin States of Bioinorganic Complexes from Nickel L-Edge X-Ray Absorption and Resonant Inelastic X-Ray Scattering. *J. Phys. Chem. C* **2013**, *117* (47), 24767−24772.
(18) Wang, H.; Ralston, C. Y.; Patil, D. S.; Jones, R. M.; Gu, W.; Verhagen, M.; Adams, M.; Ge, P.; Riordan, C.; Marganian, C. A.; Mascharak, P.; Kovacs, J.; Miller, C. G.; Collins, T. J.; Brooker, S.; Croucher, P. D.; Wang, K.; Stiefel, E. I.; Cramer, S. P. Nickel L-Edge Soft X-Ray Spectroscopy of Nickel−Iron Hydrogenases and Model Compounds - Evidence for High-Spin Nickel(II) in the Active Enzyme. *J. Am. Chem. Soc.* **2000**, *122* (43), 10544−10552.
(19) Wang, H.; Ge, P.; Riordan, C. G.; Brooker, S.; Woomer, C. G.; Collins, T.; Melendres, C. A.; Graudejus, O.; Bartlett, N.; Cramer, S. P. Integrated X-Ray L Absorption Spectra. Counting Holes in Ni Complexes. *J. Phys. Chem. B* **1998**, *102* (42), 8343−8346.
(20) Sreekantan Nair Lalithambika, S.; Golnak, R.; Winter, B.; Atak, K. Electronic Structure of Aqueous $[Co(bpy)_3]^{2+/3+}$ Electron Mediators. *Inorg. Chem.* **2019**, *58* (8), 4731−4740.
(21) Hong, J.; Fauvell, T. J.; Helweh, W.; Zhang, X.; Chen, L. X. Investigation of the Photoinduced Axial Ligation Process in the Excited State of Nickel(II) Phthalocyanine. *J. Photochem. Photobiol. Chem.* **2019**, *372*, 270−278.
(22) Avakyan, L. A.; Manukyan, A. S.; Mirzakhanyan, A. A.; Sharoyan, E. G.; Zubavichus, Y. V.; Trigub, A. L.; Kolpacheva, N. A.; Bugaev, L. A. Atomic Structure of Nickel Phthalocyanine Probed by X-Ray Absorption Spectroscopy and Density Functional Simulations. *Opt. Spectrosc.* **2013**, *114* (3), 347−352.
(23) Colpas, G. J.; Maroney, M. J.; Bagyinka, C.; Kumar, M.; Willis, W. S.; Suib, S. L.; Mascharak, P. K.; Baidya, N. X-Ray Spectroscopic Studies of Nickel Complexes, with Application to the Structure of Nickel Sites in Hydrogenases. *Inorg. Chem.* **1991**, *30* (5), 920−928.
(24) Hocking, R. K.; Solomon, E. I. Ligand Field and Molecular Orbital Theories of Transition Metal X-Ray Absorption Edge Transitions. In *Molecular Electronic Structures of Transition Metal Complexes I*; Mingos, D. M. P., Day, P., Dahl, J. P., Eds.; Springer: Berlin, 2012; pp 155−184. DOI: 10.1007/430_2011_60.
(25) Ottenwaelder, X.; Aukauloo, A.; Journaux, Y.; Carrasco, R.; Cano, J.; Cervera, B.; Castro, I.; Curreli, S.; Muñoz, M. C.; Roselló, A. L.; Soto, B.; Ruiz-García, R. Synthesis, Structure, Spectroscopy and Redox Chemistry of Square-Planar Nickel(II) Complexes with Tetradentate o-Phenylenedioxamidates and Related Ligands. *Dalton Trans.* **2005**, *15*, 2516.
(26) Gu, W.; Wang, H.; Wang, K. Nickel L-Edge and K-Edge X-Ray Absorption Spectroscopy of Non-Innocent $Ni[S_2C_2(CF_3)_2]_2^n$ Series (n = − 2, − 1, 0): Direct Probe of Nickel Fractional Oxidation State Changes. *Dalton Trans.* **2014**, *43* (17), 6406−6413.
(27) Klein, A.; Kaiser, A.; Wielandt, W.; Belaj, F.; Wendel, E.; Bertagnolli, H.; Záliš, S. Halide Ligands—More Than Just σ-Donors? A Structural and Spectroscopic Study of Homologous Organonickel Complexes. *Inorg. Chem.* **2008**, *47* (23), 11324−11333.
(28) Feth, M. P.; Klein, A.; Bertagnolli, H. Investigation of the Ligand Exchange Behavior of Square-Planar Nickel(II) Complexes by X-Ray Absorption Spectroscopy and X-Ray Diffraction. *Eur. J. Inorg. Chem.* **2003**, *2003* (5), 839−852.
(29) Shreiber, S. T.; DiMucci, I. M.; Khrizanforov, M. N.; Titus, C. J.; Nordlund, D.; Dudkina, Y.; Cramer, R. E.; Budnikova, Y.; Lancaster, K. M.; Vicic, D. A. $[(MeCN)Ni(CF_3)_3]^-$ and $[Ni(CF_3)_4]^{2-}$: Foundations toward the Development of Trifluoromethylations at Unsupported Nickel. *Inorg. Chem.* **2020**, *59* (13), 9143−9151.
(30) Sutcliffe, E.; Cagan, D. A.; Hadt, R. G. Ultrafast Photophysics of Ni(I)−Bipyridine Halide Complexes: Spanning the Marcus Normal and Inverted Regimes. *J. Am. Chem. Soc.* **2024**, *146* (22), 15506−15514.
(31) Kroll, T.; Baker, M. L.; Wilson, S. A.; Lundberg, M.; Juhin, A.; Arrio, M.-A.; Yan, J. J.; Gee, L. B.; Braun, A.; Weng, T.-C.; Sokaras, D.; Hedman, B.; Hodgson, K. O.; Solomon, E. I. Effect of 3d/4p Mixing on 1s2p Resonant Inelastic X-Ray Scattering: Electronic Structure of Oxo-Bridged Iron Dimers. *J. Am. Chem. Soc.* **2021**, *143* (12), 4569−4584.
(32) Baker, M. L.; Mara, M. W.; Yan, J. J.; Hodgson, K. O.; Hedman, B.; Solomon, E. I. K- and L-Edge X-Ray Absorption Spectroscopy (XAS) and Resonant Inelastic X-Ray Scattering (RIXS) Determination of Differential Orbital Covalency (DOC) of Transition Metal Sites. *Coord. Chem. Rev.* **2017**, *345*, 182−208.
(33) Obeng, A.; Autschbach, J. How Much Electron Donation Is There In Transition Metal Complexes? A Computational Study. *J. Chem. Theory Comput.* **2024**, *20*, 4965.
(34) Harvey, J. N. On the Accuracy of Density Functional Theory in Transition Metal Chemistry. *Annu. Rep. Sect. C: Phys. Chem.* **2006**, *102*, 203−226.
(35) Hocking, R. K.; Wasinger, E. C.; de Groot, F. M. F.; Hodgson, K. O.; Hedman, B.; Solomon, E. I. Fe L-Edge XAS Studies of $K_4[Fe(CN)_6]$ and $K_3[Fe(CN)_6]$: A Direct Probe of Back-Bonding. *J. Am. Chem. Soc.* **2006**, *128* (32), 10442−10451.
(36) Pettersson, L. G. M.; Hatsui, T.; Kosugi, N. Ni 2p−3d Photoabsorption and Strong Charge Transfer Satellites in Divalent Ni Complexes with Molecular Ligands. Evaluation of p-Back Donation Based on the Density Functional Theory Approach. *Chem. Phys. Lett.* **1999**, *311* (3−4), 299−305.
(37) Hatsui, T.; Takata, Y.; Kosugi, N. Strong Metal-to-Ligand Charge Transfer Bands in Ni 2p Photoabsorption of $K_2Ni(CN)_4$·H2O. *Chem. Phys. Lett.* **1998**, *284* (5), 320−324.
(38) Koroidov, S.; Hong, K.; Kjaer, K. S.; Li, L.; Kunnus, K.; Reinhard, M.; Hartsock, R. W.; Amit, D.; Eisenberg, R.; Pemmaraju, C. D.; Gaffney, K. J.; Cordones, A. A. Probing the Electron Accepting Orbitals of Ni-Centered Hydrogen Evolution Catalysts with Non-innocent Ligands by Ni L-Edge and S K-Edge X-Ray Absorption. *Inorg. Chem.* **2018**, *57* (21), 13167−13175.
(39) Wallick, R.; Chakrabarti, S.; Burke, J.; Gnewkow, R.; Chae, J. B.; Rossi, T.; Mantouvalou, I.; Kanngieer, B.; Fondell, M.; Eckert, S.; Dykstra, C.; Smith, L.; Vura-Weis, J.; Mirica, L.; Veen, R. V. der. Excited-State Identification of a Nickel-Bipyridine Photocatalyst by Time-Resolved X-ray Absorption Spectroscopy. *J. Phys. Chem. Lett.* **2024**, *15* (18), 4976−4982.
(40) Hatsui, T.; Kosugi, N. Metal-to-Ligand Charge Transfer in Polarized Metal L-Edge X-Ray Absorption of Ni and Cu Complexes. *J. Electron Spectrosc. Relat. Phenom.* **2004**, *136* (1), 67−75.
(41) Krasnikov, S. A.; Preobrajenski, A. B.; Sergeeva, N. N.; Brzhezinskaya, M. M.; Nesterov, M. A.; Cafolla, A. A.; Senge, M. O.; Vinogradov, A. S. Electronic Structure of Ni(II) Porphyrins and Phthalocyanine Studied by Soft X-Ray Absorption Spectroscopy. *Chem. Phys.* **2007**, *332* (2), 318−324.
(42) Biasin, E.; Nascimento, D. R.; Poulter, B. I.; Abraham, B.; Kunnus, K.; Garcia-Esparza, A. T.; Nowak, S. H.; Kroll, T.; Schoenlein, R. W.; Alonso-Mori, R.; Khalil, M.; Govind, N.; Sokaras, D. Revealing the Bonding of Solvated Ru Complexes with Valence-to-Core Resonant Inelastic X-Ray Scattering. *Chem. Sci.* **2021**, *12* (10), 3713−3725.

https://doi.org/10.1021/acs.jpclett.4c02917
J. Phys. Chem. Lett. 2025, 16, 87−94

(43) Lu, Y.; Höppner, M.; Gunnarsson, O.; Haverkort, M. W. Efficient Real-Frequency Solver for Dynamical Mean-Field Theory. *Phys. Rev. B* **2014**, *90* (8), No. 085102.
(44) Haverkort, M. W.; Zwierzycki, M.; Andersen, O. K. Multiplet Ligand-Field Theory Using Wannier Orbitals. *Phys. Rev. B* **2012**, *85* (16), No. 165113.
(45) Haverkort, M. W.; Sangiovanni, G.; Hansmann, P.; Toschi, A.; Lu, Y.; Macke, S. Bands, Resonances, Edge Singularities and Excitons in Core Level Spectroscopy Investigated within the Dynamical Mean-Field Theory. *Europhys. Lett.* **2014**, *108* (5), 57004.
(46) Haverkort, M. W. *Quanty* for Core Level Spectroscopy - Excitons, Resonances and Band Excitations in Time and Frequency Domain. *J. Phys. Conf. Ser.* **2016**, *712*, No. 012001.
(47) de Groot, F. M. F.; Elnaggar, H.; Frati, F.; Wang, R.; Delgado-Jaime, M. U.; van Veenendaal, M.; Fernandez-Rodriguez, J.; Haverkort, M. W.; Green, R. J.; van der Laan, G.; Kvashnin, Y.; Hariki, A.; Ikeno, H.; Ramanantoanina, H.; Daul, C.; Delley, B.; Odelius, M.; Lundberg, M.; Kuhn, O.; Bokarev, S. I.; Shirley, E.; Vinson, J.; Gilmore, K.; Stener, M.; Fronzoni, G.; Decleva, P.; Kruger, P.; Retegan, M.; Joly, Y.; Vorwerk, C.; Draxl, C.; Rehr, J.; Tanaka, A. 2p X-Ray Absorption Spectroscopy of 3d Transition Metal Systems. *J. Electron Spectrosc. Relat. Phenom.* **2021**, *249*, No. 147061.
(48) Retegan, M.; Kuschel, S. Mretegan/Crispy: V0.7.4, 2023. DOI: 10.5281/zenodo.7784033.
(49) Hoffmann, R.; Alvarez, S.; Mealli, C.; Falceto, A.; Cahill, T. J. I.; Zeng, T.; Manca, G. From Widely Accepted Concepts in Coordination Chemistry to Inverted Ligand Fields. *Chem. Rev.* **2016**, *116* (14), 8173−8192.
(50) Stiefel, E. I.; Waters, J. H.; Billig, E.; Gray, H. B. The Myth of Nickel(III) and Nickel(IV) in Planar Complexes. *J. Am. Chem. Soc.* **1965**, *87* (13), 3016−3017.
(51) Steen, J. S.; Knizia, G.; Klein, J. E. M. N. σ-Noninnocence: Masked Phenyl-Cation Transfer at Formal Ni^{IV}. *Angew. Chem., Int. Ed.* **2019**, *58* (37), 13133−13139.
(52) Budnikova, Y. H.; Vicic, D. A.; Klein, A. Exploring Mechanisms in Ni Terpyridine Catalyzed C−C Cross-Coupling Reactions—A Review. *Inorganics* **2018**, *6* (1), 18.
(53) Kaim, W. The Shrinking World of Innocent Ligands: Conventional and Non-Conventional Redox-Active Ligands. *Eur. J. Inorg. Chem.* **2012**, *2012* (3), 343−348.
(54) Kaim, W.; Schwederski, B. Non-Innocent Ligands in Bioinorganic Chemistry—An Overview. *Coord. Chem. Rev.* **2010**, *254* (13), 1580−1588.
(55) Ciszewski, J. T.; Mikhaylov, D. Y.; Holin, K. V.; Kadirov, M. K.; Budnikova, Y. H.; Sinyashin, O.; Vicic, D. A. Redox Trends in Terpyridine Nickel Complexes. *Inorg. Chem.* **2011**, *50* (17), 8630−8635.
(56) Dawson, G. A.; Lin, Q.; Neary, M. C.; Diao, T. Ligand Redox Activity of Organonickel Radical Complexes Governed by the Geometry. *J. Am. Chem. Soc.* **2023**, *145* (37), 20551−20561.
(57) Cremer, D.; Kraka, E. Generalization of the Tolman Electronic Parameter: The Metal−Ligand Electronic Parameter and the Intrinsic Strength of the Metal−Ligand Bond. *Dalton Trans.* **2017**, *46* (26), 8323−8338.
(58) Cagan, D. A.; Bim, D.; McNicholas, B. J.; Kazmierczak, N. P.; Oyala, P. H.; Hadt, R. G. Photogenerated Ni(I)−Bipyridine Halide Complexes: Structure−Function Relationships for Competitive C-(sp2)−Cl Oxidative Addition and Dimerization Reactivity Pathways. *Inorg. Chem.* **2023**, *62*, 9538−9551.

NOTE ADDED AFTER ASAP PUBLICATION

This paper was published ASAP on December 19, 2024, with an incorrect ref 30. This was corrected in the version published on January 9, 2025.

https://doi.org/10.1021/acs.jpclett.4c02917
J. Phys. Chem. Lett. 2025, 16, 87−94